Ceramics International 49 (2023) 32779–32788

Contents lists available at ScienceDirect

Ceramics International

journal homepage: www.elsevier.com/locate/ceramint

Functional properties of transparent ZnO thin films synthetized by using spray pyrolysis for environmental and biomedical applications

J.G. Cuadra [a,*], Ana C. Estrada [b], C. Oliveira [c], L.A. Abderrahim [a], S. Porcar [a], D. Fraga [a], T. Trindade [b], M.P. Seabra [d], J. Labrincha [d], J.B. Carda [a]

[a] Department of Inorganic and Organic Chemistry, Universitat Jaume I, Avda. Sos Baynat S/n, 12071, Castelló de La Plana, Spain
[b] Department of Chemistry, CICECO-Aveiro Institute of Materials, University of Aveiro, 3810-193, Aveiro, Portugal
[c] Department of Biology, CESAM, University of Aveiro, Campus Universitário de Santiago, 3810-193, Aveiro, Portugal
[d] Materials and Ceramic Engineering Department, CICECO, University of Aveiro, Campus Universitário de Santiago, 3810-193, Aveiro, Portugal

ARTICLE INFO

Handling editor: Dr P. Vincenzini

ABSTRACT

Spray pyrolysis is a promising method for producing thin, transparent films on glass substrates. ZnO thin films synthesized by this method exhibit high crystallinity, adhesion and chemical resistance. They also possess the ability to degrade water pollutants and exhibit antibacterial properties under UV light. The crystalline structure of these films has been studied using grazing X-ray diffraction (GIXRD), atomic force microscopy (AFM) and scanning electron microscopy (SEM), while transmission electron microscopy (TEM) has been used to investigate their composition and purity. Other techniques such as X-ray photoelectron spectroscopy (XPS), Raman spectroscopy and ultraviolet–visible spectroscopy were also employed. ICP-OES was used to evaluate photocatalyst leaching. These transparent thin films have exceptional optical properties, with a transmittance of 95%. The photocatalytic degradation of 4-Nitrophenol (4-NP) by ZnO thin films showed a degradation rate of 94% in 270 min with a kinetic constant value of 3.1×10^{-3} mM/min. The films are also highly durable and reusable, exhibiting superior performance compared to other ZnO photocatalysts. The bactericidal activity of these transparent films was also evaluated, with a value of 60.6% being obtained using *Escherichia coli* after irradiating the films with UV light for 3 h.

1. Introduction

In recent years, materials transparency has become a very important aspect in several fields such as optics and photonics [1,2], architecture and construction [2,3], electronics [4,5], medicine [6,7] or aerospace and defence [8,9]. Transparent materials thus play a crucial role in many areas of modern technology and industry, and their continued development and improvement are essential to advance in these fields [10]. Zinc oxide (ZnO) is among the most researched materials that become transparent, and consequently it is also one of the most widely used oxides in photocatalysis [11,12], photovoltaic cells [13,14], piezoelectrics [15,16], sensors [17,18], antibacterial agents [19,20] or fungicides [21,22]. ZnO belongs to the n-type semiconductor with an exciton binding energy of 60 meV and a direct band gap of 3.37 eV.This bandgap value indicates its high UV absorption and its transparency towards the visible range [23,24]. Reactive oxygen species (ROS) such as superoxide anion ($O_2^{\bullet}$), hydroxyl radical (OH•) and singlet oxygen ($^1O_2$) are able to degrade different types of organisms such as gram-positive and gram-negative bacteria [25,26] and cancer cells [27] by inducing oxidative stress [28,29], as well as promoting the degradation of water pollutants [30]. Some of the substances described as water pollutants by the European Chemical Agency (ECHA) [31] are pharmaceuticals [32], pesticides [33], personal care products (PCPs) [34] or industrial by-products [35]. Moreover, there is a wide variety of morphologies thanks to the different methods of ZnO synthesis, whether in the form of nanoparticles (NPs) [36], nanotubes (NTs) [37], nanowires (NWs) [38] or thin films [39]. The use of ZnO NPs as bactericidal agents is well known, with particle size, smaller particles generally having a higher surface area-to-mass ratio, which can enhance their reactivity and potentially lead to increased ROS [40]. However, ZnO NPs and NTs used as antibacterial agents or photocatalysts for pollutants in water have serious limitations, especially when used to functionalize a surface. First, NPs tend to aggregate, leading to a decrease in their antibacterial capability [41]. Although aggregation is discussed in the

* Corresponding author.
E-mail address: jcuadra@uji.es (J.G. Cuadra).

https://doi.org/10.1016/j.ceramint.2023.07.246
Received 26 June 2023; Received in revised form 21 July 2023; Accepted 27 July 2023
Available online 2 August 2023

context of NPs, this phenomenon also occurs in a large number of nanostructured materials, due to the strong interaction that NPs undergo in relation to their size, shape, surface charge or pH of the medium in which they are dispersed [42,43]. Another major challenge in the use of ZnO NPs is their relatively low stability in aqueous solutions, which limits their application as photocatalysts for surfaces that may come into contact with water [44–46]. For the generation of surfaces with antimicrobial properties, it is mandatory to ensure that ZnO NPs are firmly attached to the surface and that they are not released over time.

A multitude of methods are available to obtain transparent thin films, such as atomic layer deposition (ALD) [47], chemical vapour deposition (CVD) [48], electroplating [49] or sol-gel spin coating [50]. In all these techniques the adaptation to industrial applications is severely limited because they require high levels of technical sophistication or the creation of a high vacuum for the production of thin films [51]. However, the spray pyrolysis method has no such drawbacks because it is able to produce transparent thin films by simply spraying a precursor solution of the material onto the heated substrate. Moreover, it can be used on a multitude of substrates, including glass [52], metal or polymer [53], which is advantageous for industrial applications.

In this work, the deposition of ZnO on glass to form a thin transparent film has been achieved using the spray pyrolysis method. The transparent ZnO thin films exhibit high crystallinity and adhesion to glass substrates, as well as high resistance in neutral and basic aqueous media. The study of this material as a photocatalyst was also carried out using a UV lamp, revealing that it has a high capacity for the photodegradation of a pollutant such as 4-NP. In addition, it was demonstrated that these thin films, when exposed to this type of light, can function as antibacterial surfaces.

2. Experimental section

2.1. Chemicals

Zinc acetate ($Zn(CH_3COO)_2\bullet\ 2H_2O \geq$ 99.5% PanReac AppliChem, ethanol (EtOH, Scharlau), ammonia (NH_3, 30% w/w, PanReactAppliChem), 4-nitrophenol (4-NP, ≥98%, Sigma-Aldrich), sodium hydroxide (NaOH, pearls 1–2 mm, ≥98%, Labkem), hydrochloric acid (HCl, 37%, PanReactAppliChem) and deionized water, with pH 7.1 ± 0.2 and a resistivity of 17.9 MΩ-cm (Ultramatic Plus, Wasserlab, Spain) were used. *Tert*-butyl alcohol (t-BuOH), formic acid (HCOOH) and 1,4-Benzoquinone ($C_6H_4O_2$) (99%, purity) were purchased from Sigma-Aldrich.

2.2. Instrumentation

The transparent ZnO thin films were examined to determine their crystalline structure using grazing incidence X-ray diffraction (GIXRD). To conduct the analysis, a Cu K radiation source-equipped Burker-ASX X-ray diffractometer, specifically the D4 Endeavour model, was employed. The scanning process involved stepping from 10° to 90° 2θ, with a step size of 0.05° 2θ and a counting duration of 3 s per step. The incident angle of the measurements, approximately 1°, was determined experimentally. For the investigation of surface characteristics, morphology, and thickness of the coatings, scanning electron microscopy (SEM) was performed using a JEOL 7001 F instrument. SEM-EDS mappings were obtained using an acceleration voltage of 10 kV and a beam current of 0.6 nA. To ensure accurate spectral recordings, drift correction was applied, with a step size of 0.3 μm and a minimal dwell time of 0.3 msec. The EDS analyses were conducted using Aztec 4.3 software developed by Oxford Instruments in the United Kingdom. To measure the thickness of the layers, micrographs of cross-sections were utilized. The crystallite sizes were determined by applying the Debye-Scherrer equation (Equation (1)) to the XRD data [52].

$$\mathbf{D} = \frac{\mathbf{k}\lambda}{\beta\ \mathbf{cos}\ \theta} \tag{1}$$

The Debye-Scherrer equation (Equation (1)) utilizes various parameters to determine the crystallite sizes. In the equation, the Scherrer constant (k) is typically 0.9 for spherical particles, the X-ray wavelength (λ) is 1.5405 Å, the peak width at half-maximum (β) represents the width of the peak at half of its maximum intensity, and θ corresponds to the Bragg diffraction angle [55]. To examine the surfaces of the transparent thin films, an atomic force microscopy (AFM) operating in contact mode was used. Specifically, a JSPM-5200 JEOL Scanning Probe Microscope was used for this purpose. For Transmission Electron Microscopy (TEM), a JEOL JEM-1010 EM-24830 FLASH digital camera equipped with a CMOS sensor was utilized. This camera offers a resolution of 2k × 2k and facilitated the TEM analysis. The microscope also featured an Oxford STEM DF/BF image acquisition system with a drift silicon sensor, an 80 mm^2 window and 127 eV resolution for the Mn K line. Before TEM analysis, a drop (8 μL) of a suspension of the removed thin film diluted in ethanol was deposited on a copper grid with an amorphous carbon film and allowed to dry. The thin film's composition and purity were examined using X-ray photoelectron spectroscopy (XPS) on a Sage 150 photoelectron spectrometer, which is part of a multi-technique surface analysis system. The electron-energy detection was performed using a Mac 2 Cameca Riber double stage cylindrical mirror detector. The X-ray source utilized was a dual anode Cameca SCX700. In all cases, a non-monochromatic Al K X-ray source (energy = 1486.6 eV) was employed for excitation. Raman scattering measurements were carried out using a Hobiba Jobin-Yvon FHR-640 monochromator coupled with a CCD detector in a backscattering configuration. Gas (325 nm) and solid-state (532 nm) lasers with respective power densities ~10 and ~50 W/cm^2 were used to excite the samples. The spectral alignment was adjusted by setting the primary peak of a monocrystalline silicon sample to 520 cm-1. Diffuse reflectance spectroscopy (DRS) was conducted on a UV–Vis spectrophotometer (JASCO U-560). The spectra of the materials were obtained using a Bruker Optics Tensor 27 spectrometer connected to a horizontal attenuated total reflectance (ATR) cell, with 256 scans performed at a resolution of 4 cm^{-1}. To analyze the leaching of the photocatalyst, a Jobin Yvon Activa M ICP-OES instrument was utilized.

The optical bandgap value for the thin film was derived from the absorption coefficient (α) value, which was calculated using Lambert's Law in the following Equation (2) [53]:

$$\mathbf{A} = \frac{\mathbf{1}}{\mathbf{t}}\ \mathbf{ln}\left(\frac{\mathbf{1}}{\mathbf{T}}\right) \tag{2}$$

where T is the transmittance, and t is the film thickness. The optical bandgap of thin films could be calculated by extrapolating $(\alpha h\nu)^2$ versus $h\nu$ using Equation (3).

$$\boldsymbol{\alpha h\upsilon} = \mathbf{A}\left(\mathbf{h\upsilon} - \mathbf{E_g}\right)^{\frac{1}{2}} \tag{3}$$

where A is a constant, hv is the photon energy, and E_g is the optical bandgap.

2.3. Preparation of transparent ZnO thin films

For the preparation of the transparent ZnO thin films, 0.5 mol of Zn $(CH_3COO)_2{\cdot}2H_2O$ were dissolved in EtOH (40 mL). This mixture of precursors was stirred for 1 h to ensure the homogeneity of the solution. Using a 100 mL capacity atomizer with a fine grade of spraying (CAT NUMBER: 34 48 51) connected to a compressed air pump at a pressure of 0.9 bar (Fig. S1), transparent thin coatings were manually deposited onto a soda-lime glass (2.5 × 2.5 cm) previously heated to 400 °C (Fig. 1). Prior to heating, the glass was cleansed in a 30% (w/w) NH_3 solution followed by ultrasonication for 15 min. The deposited thin

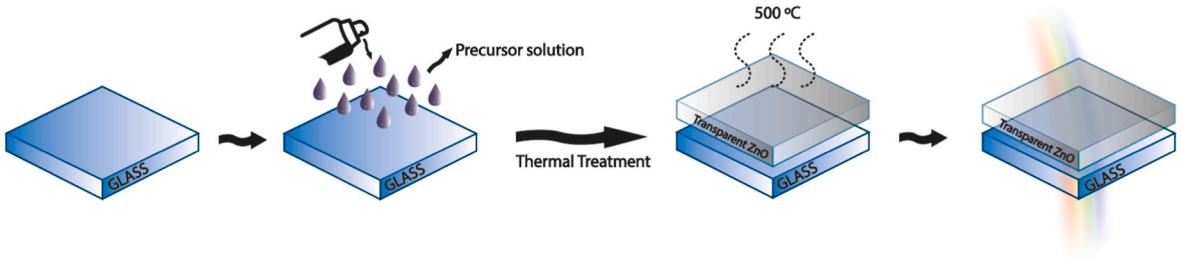

Fig. 1. Schematic representation of the preparation of transparent ZnO thin films on glass substrates.

coatings were then heated to 500 °C on a hot plate under atmospheric pressure to remove any organic residue. Fig. S2 shows the appearance of the transparent ZnO thin films on the glass substrate.

2.4. Experiments for the screening of photocatalytic activity

The photocatalytic efficiency of the ZnO thin film was examined for its ability to degrade 4-Nitrophenol (4-NP) under UV light exposure at room temperature. In a typical procedure, the samples were immersed in a glass vessel containing 30 mL of an aqueous solution of 4-NP (6.95 mg/L). Prior to irradiation, the solution was left in darkness for 30 min to establish an adsorption/desorption equilibrium. A UV light source (SUPRATECH HTC 150–211 UV, Osram) with a nominal power rating of 150 W, emitting 22 W in the UVA region (315–400 nm) and 6 W in the UVB region (280–315 nm), was employed. The light intensity measured was 0.105 W/cm^2. Refer to Fig. S3 for a depiction of the experimental setup for the photocatalysis. At regular intervals, samples of the reaction mixture were withdrawn, and a NaOH pellet was promptly added to each of them to induce the formation of 4-nitrophenolate ions, which exhibit maximum absorption at 410 nm (Fig. S4). The concentration of 4-NP was monitored using UV–Vis spectroscopy at 410 nm, employing Equation (4):

$$\eta\,(\%) = \left(1 - \frac{C_t}{C_0}\right) \times 100 \tag{4}$$

where C_0 represents the initial 4-NP concentration and Ct refers to the real-time concentrations of 4-NP, respectively. The kinetics of 4-NP were performed using the expression presented in Equation (5):

$$k_{app} = -\frac{C - C_0}{t} \tag{5}$$

where k_{app} (mM/min) represents the reaction rate constant in mM at time t (min).

To determine the stability of the as-prepared ZnO thin film, it was recovered and subjected to four additional photodegradation cycles under the same conditions. To clarify the photocatalytic reaction mechanism, the degradation of 4-NP was carried out in the presence of 1 mM of *tert*-butyl alcohol (t-BuOH), formic acid (FA), and 1,4-Benzoquinone (1,4-BQ), which are known as scavenger species, for capturing hydroxyl radicals ($OH^{\bullet}$), holes (h^+) and superoxide radicals ($O2^{-\bullet}$), respectively [54,55].

2.5. Determination of antibacterial activity

The antibacterial activity of ZnO thin films was evaluated using a modified version of the standard method test Jisz 2801_2000 as described previously [56]. Briefly, *Escherichia coli* ATCC 25922 cells were used to test for the antibacterial activity of ZnO thin films with or without irradiation of UV light for 3 h. As a reference, glass samples were used. At least 2 sample pieces for each condition were used and 3 plates per sample were cultivated to determine the concentration of colony-forming units (CFU/mL) in each assayed condition.

The antibacterial rate (R) was calculated according to Equation (6):

$$(R) = (N_0 - N) / N_0 \times 100 \tag{6}$$

where N_0 represents the average number of viable bacteria on a reference sample, and N is the average number of bacteria on tested samples.

3. Results and discussion

3.1. Characterization of transparent ZnO thin films

The microstructure of ZnO thin films, such as crystalline orientation, crystalline structure, uniformity, and film density, was studied. The orientation and structure of ZnO crystals were analyzed based on GIXRD patterns. Seven diffraction peaks were identified in the GIXRD pattern, indicating a polycrystalline structure, as shown in Fig. 2(a). The most intense diffraction peak (002) indicates that the crystallites are predominantly oriented perpendicular to the glass substrate on which they have been deposited. Using thin film deposition techniques, crystalline growth is predominant along the z-axis due to the reduced surface energy of the (002) plane [57]. Furthermore, the computed values for the lattice constants a and c were determined to be 3.24 Å and 5.21 Å.The ratio of c to a (c/a) was found to be 1.602, which closely approximates the c/a ratio observed in a hexagonal structure (c/a = 1.633). Hence, the values are in accordance with those indicated in the standard card (JCPDS 070–2551) for ZnO, wurtzite type. The mean particle size (D) of the ZnO thin films, estimated to be 25.0 nm, was calculated using the Scherrer equation based on the diffraction peak at$2\theta = 34.4^{\circ}$ associated with the (002) reflection plane. AFM images reveal that the surface of these thin films is rough, with a root-mean-square (RMS) roughness of 29.9 nm and an average roughness (AR) of 24.4 nm. The RMS value obtained is comparable to values obtained on SiO_2/Si substrates [60], and the average particulate size of ZnO in the layer corresponds to the value estimated by Sherrer's formula. Fig. 2(c) shows the top view, and Fig. 2(d) shows the cross-sectional view of the ZnO thin films. The top view SEM image (Fig. 2(c)) confirms the formation of a dense layer, consisting of flawlessly sintered round grains. In addition, the cross-sectional SEM image shows that ZnO has a dense columnar structure and that its adhesion to the glass substrate is strong and delamination-free (Fig. 2(d)). Fig. S5 shows the transmission electron microscopy of a selective area, confirming that ZnO crystals grew perpendicular to the glass. The interplanar distance calculated from Fig. S5 is 0.26 nm, which is consistent with the interplanar distance of the (002) plane of ZnO (JCPDS 070–2551). EDS analysis shows that the transparent thin film is composed exclusively of ZnO.

The Raman spectrum of a ZnO thin film measured under a 325 nm excitation wavelength, showing the vibrational modes, is presented in Fig. 3. Under resonant conditions, the intense LO peak (sum of two modes with A1 (LO) and E1 (LO) symmetry) and a second-order 2LO peak are observed in ZnO thin films [58]. These additional low-intensity peaks can be identified (see the vertical dashed lines in Fig. 3). They all are associated with the fundamental or previously identified multi-phonon modes of crystalline ZnO [59]. No additional peaks/bands that could be associated with the presence of other metals or impurities were visible. XPS was used to confirm the presence of Zn, O and C. The

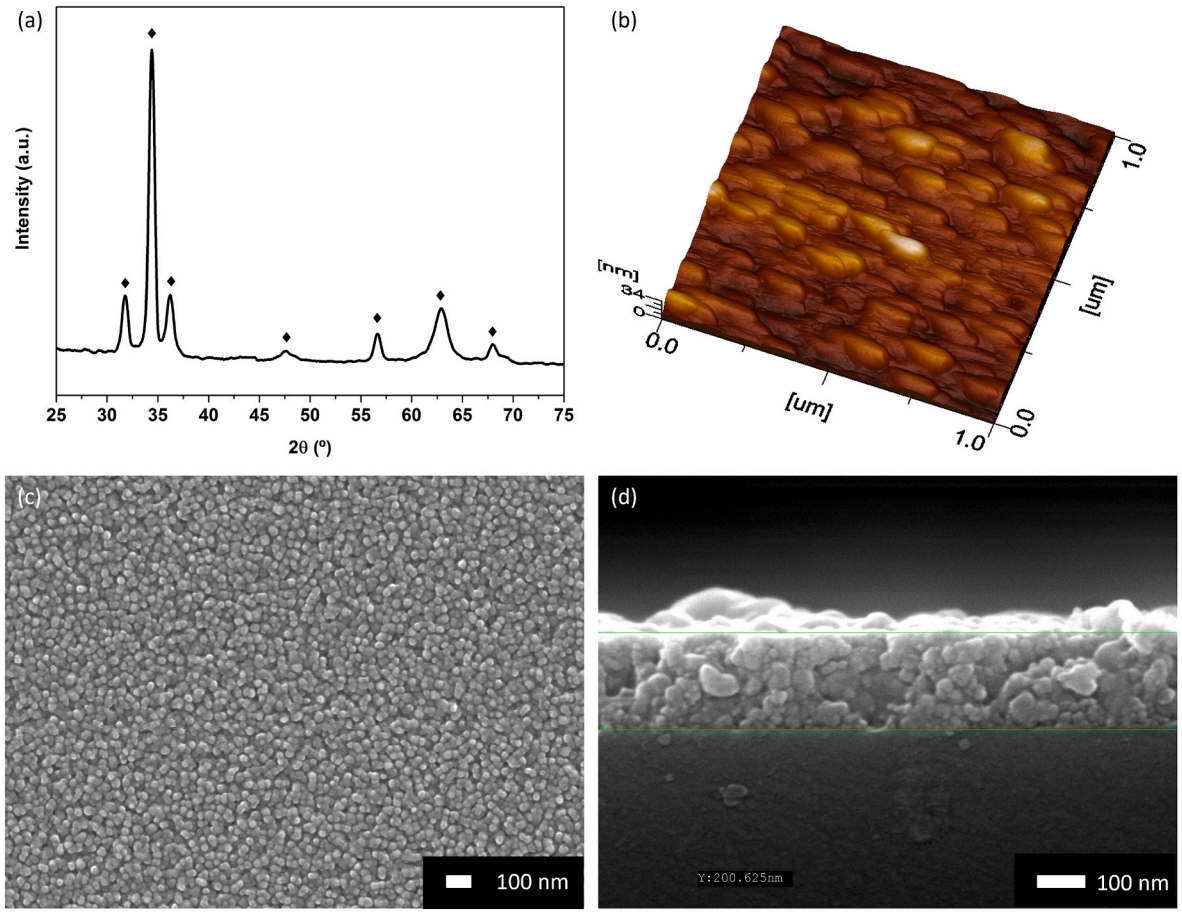

Fig. 2. (A) GIXRD pattern, (b) AFM image, (c) top SEM image, and (d) cross-sectional SEM image of transparent ZnO thin films.

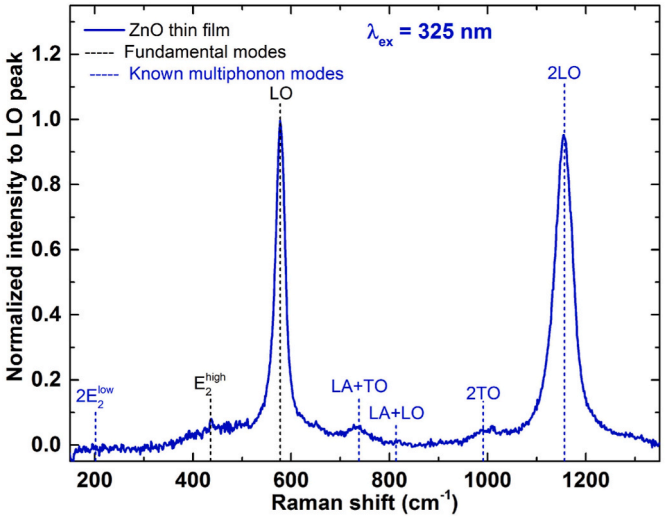

Fig. 3. Raman spectrum of a typical ZnO thin film (laser line at 325 nm).

characteristic peaks of Zn 2p (1021 eV), O 1s (530 eV) and C 1s (285 eV) are shown in Fig. S6, quantifying the atomic content of the transparent thin film as 54.2, 42.6 and 3.3% of Zn, O and C, respectively.

As shown in Fig. 4, the transparent ZnO thin films exhibit high absorbance below 350 nm and high transmittance, reaching approximately 95% above 350 nm, i.e. across all the visible range. Fig. S3 shows the high transparency of ZnO thin films deposited on glass. The optical band gap value was estimated using the interpolation of the Tauc plot with respect to the x-axis. As shown in Fig. 3(b), the estimated value was 3.28 eV. The estimated values agree with the latest reported values for ZnO thin films [60,61].

3.2. Photocatalytic degradation of 4-NP

Initially, the photodegradation of 4-NP in the absence of ZnO thin films was evaluated in two control tests: (i) under UV-light irradiation and (ii) under UV-light irradiation with an uncoated glass substrate. The results demonstrated that only 10% of 4-NP had been degraded after 270 min in both experiments (i) and (ii) (Fig. S7). Furthermore, the capacity of the thin films to adsorb 4-NP molecules was also evaluated using ZnO thin films under dark conditions. The investigation revealed that a minute quantity of 4-NP was captured by the ZnO thin films' surface (approximately 9%), and the highest level of adsorption was attained within a 30-min interaction period, (refer to Fig. S8). Thin films had a total weight of 0.112 mg/cm^2, which is a smaller amount of catalyst as compared to related work published in the literature [62,63]. The ZnO thin films showed high photocatalytic activity, leading to 94% 4-NP degradation after 270 min, as shown in Fig. 5(a). Fig. 5(b) illustrates the difference in photodegradation efficiency by depicting the C/C_0 for the transparent ZnO thin films. The 4-NP concentration was obtained using the calibration curve presented in Fig. S9.

The kinetic profile of 4-NP degradation using the ZnO thin film is shown in Fig. 5(b), which agrees with a pseudo-zero-order reaction with a kinetic rate constant of 3.1×10^{-3} mM/min. The obtained kinetic constant for the degradation of other benzoic compounds using ZnO as a photocatalyst (Table 1) is a significantly lower value.

On the other hand, the photocatalytic degradation rate of 4-NP decreased from 94% to 33% upon addition of hydroxyl scavenger

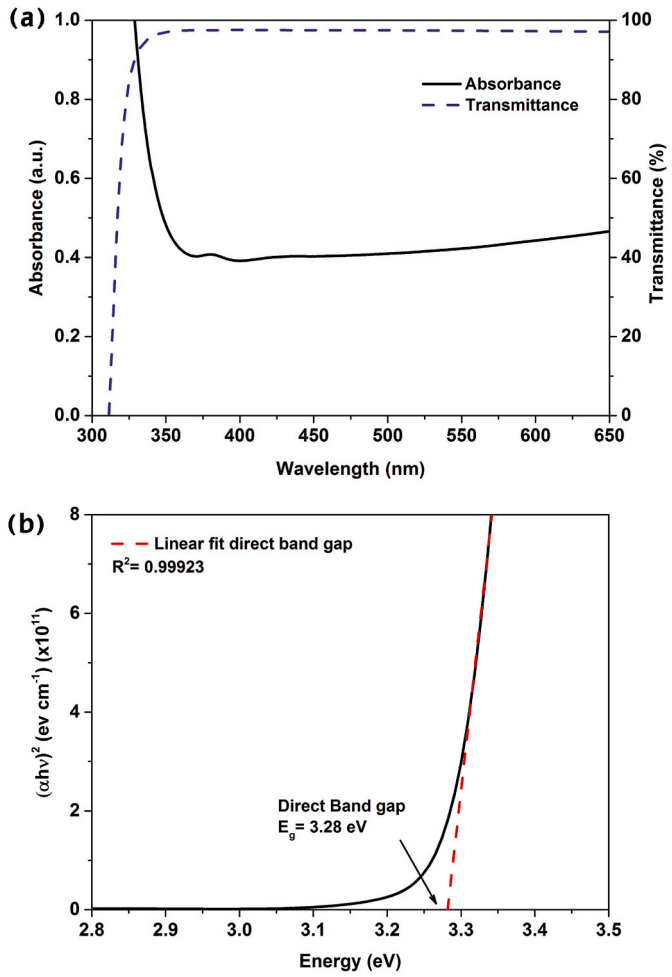

Fig. 4. The optical characteristics of the ZnO thin film, (a) the absorbance and transmittance spectra analyzed using UV–vis spectroscopy, and (b) the determination of the energy band gap through the Tauc plot.

(*tert*-butyl alcohol) to the reaction mixture, whereas addition of FA or 1,4-BQ only decreased the degradation rate to 62% and 55%, respectively (Fig. 6(a)). The bar graph in Fig. 6(b) clearly illustrates the effect of the tested scavengers on the photocatalytic degradation of 4-NP over the ZnO thin film. Fig. 6(a) and (b) show that h^+ and $O^{2-}\bullet$ exert a negligible contribution to 4-NP removal, thereby confirming the crucial role of OH• in the degradation process.

Hence, when exposed to UV light, ZnO can absorb photons and generate electron-hole pairs, which can then react with oxygen molecules to produce superoxide radicals ($O2^{-\bullet}$) and hydroxyl radicals (OH•) through the following equations 7–13 [67,68]:

$$ZnO + hv_{UV} \rightarrow ZnO + (e^- + h^+) \quad (7)$$

$$H_2O + hv_{UV} \rightarrow H^+ + OH^- \quad (8)$$

$$e^-_{CB} + O_2 \rightarrow O_2^- \quad (9)$$

$$O_2^- + H^+ \rightarrow HO_2 \quad (10)$$

$$HO_2 + e^-_{CB} \rightarrow H_2O_2 \quad (11)$$

$$H_2O_2 + e^-_{CB} \rightarrow OH^- + OH\bullet \quad (12)$$

$$OH^- + hv_{UV} \rightarrow OH\bullet \quad (13)$$

Hydroxyl radicals (OH•) formed in the equations above will attack 4-NP, producing organic radicals or other intermediates. NO_2 is formed and subsequently oxidized to NO_3 [69]. Ultimately, all parent compounds and intermediates will be oxidized into CO_2 according to the following equation (14):

$$C_6H_4OHNO_2 + 7O_2 \rightarrow 6CO_2 + H_2O + HNO_3 \quad (14)$$

Table 1
Comparison of the transparent ZnO thin films behaviour with other recently developed similar ZnO photocatalysts under UV light irradiation.

Samples	Benzoic compounds	[Pollutant] (mg/L)	Amount of photocatalyst (mg)	Removal (%)
This work	4-Nitrophenol (4-NP)	7.0	0.7	94 in 270 min
Nanocrystalline immobilized ZnO [64]	Benzoic Acid (BA)	122.1	unknown	18.3 after 400 min
ZnO powder [65]	Benzoic Acid (BA)	40.0	50	39 after 120 min
ZnO nanoparticles [66]	Tetracycline, (TC)	100.0	50	61.6 after 120 min

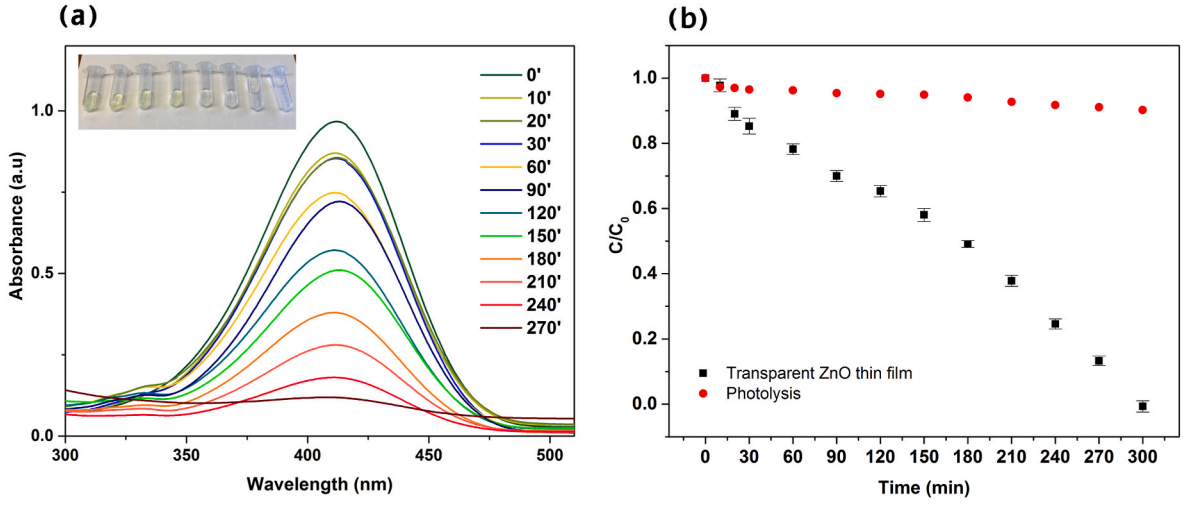

Fig. 5. (A) UV–Vis absorption spectra of aqueous solutions of 4-NP ($C_0 = 6.95$ mg/L) under UV-light irradiation in the presence of transparent ZnO thin films, and (b) pseudo-zero-order decay fitted linear regression curve for 4-NP photodegradation in the presence of transparent ZnO thin films and photolysis.

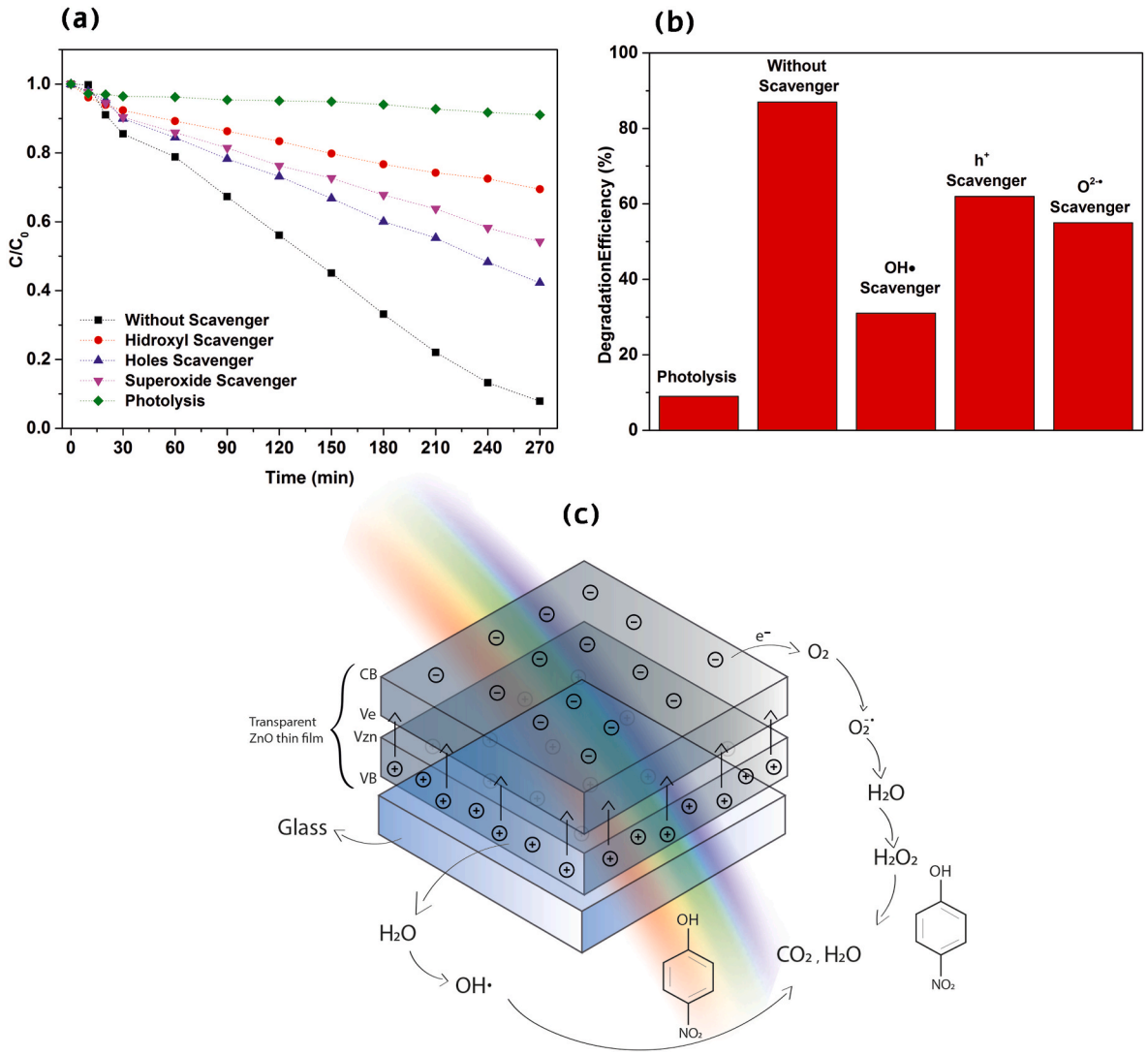

Fig. 6. (A) The kinetics of the photoreaction using different scavengers were studied on ZnO thin films that allow light to pass through (b) The percentage of degradation efficiency was evaluated using different scavengers on ZnO thin films that are transparent. (c) A visual representation illustrating the mechanism of degradation of 4-NP in the presence of transparent ZnO thin films.

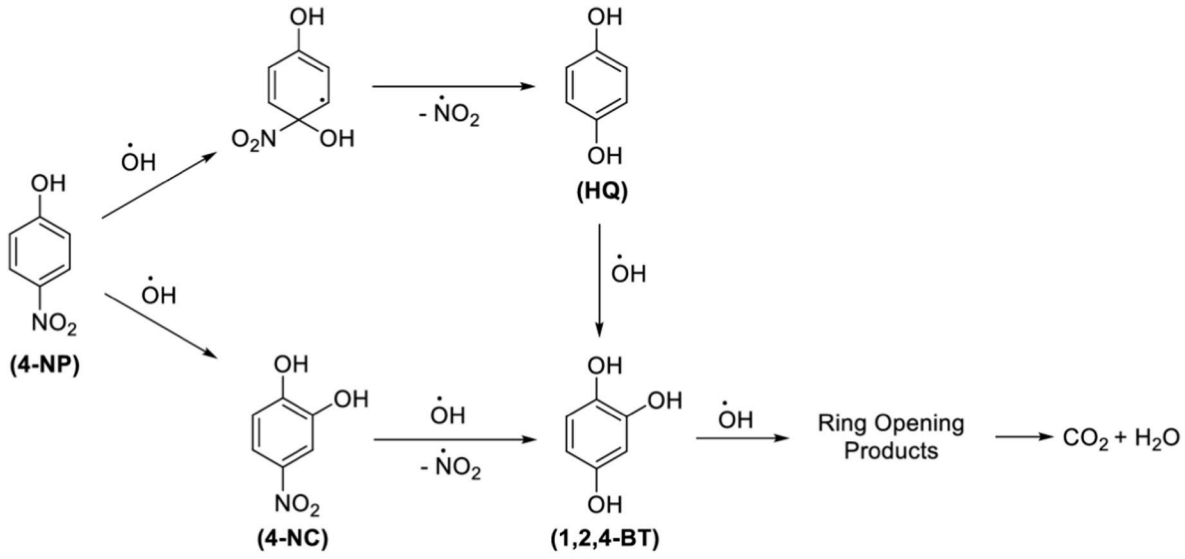

Scheme 1. Proposed reaction mechanisms of the 4-NP degradation of by hydroxyl radicals (OH•).

Alternative authors propose that the breakdown of OH• and aromatic molecules occurs through electrophilic addition instead. When 4-NP is present, ortho OH• has the ability to generate 4-nitrocatechol (4-NC). Scheme 1 illustrates a suggested sequence of reactions for the photooxidative deterioration of 4-NP. The combination of 4-NC and OH•, results in the production of 1,2,4-benzenetriol (1,2,4-BT). Subsequent reactions of primary intermediates with OH• lead to ring opening, the formation of oxygenated aliphatic compounds, and the generation of mineralization products. Hydroquinone (HQ), can be formed when OH• directly attacks the nitro group position. Similar to 4-NC, HQ reacts with OH• to yield 1,2,4-BT. The degradation of 4-NP, leading to the generation of 4-NC and HQ, and its subsequent reaction with OH• to produce 1,2,4-BT, exhibits resemblances to the degradation pathway proposed for the UV/TiO_2 photocatalytic degradation of 4-NP [70,71].

To investigate the stability and reusability of the as-prepared ZnO thin films as photocatalysts, they underwent four photocatalytic cycles (Fig. 7(a)).

In fact, high 4-NP degradation values are still observed after four cycles (90%), as indicated by the bar chart presented in Fig. S9. One of the possible explanations for this low decline is due to the adsorption of 4-NP into the active centres of the photocatalyst, which results in a slight reduction in degradation efficiency. Moreover, in order to evaluate the stability of the transparent ZnO thin films, they were immersed in different aqueous solutions at pH 1, 7 and 14 for 24 h. The presence of Zn^{2+} ions has been measured by ICP-MS in accordance with the ISO 11885 internal methodology (Table 2). The amount of Zn^{2+} in the supernatant solutions was 0.403 μg/L, which indicates the high stability of the transparent ZnO thin films in an aqueous medium. However, thin film would leach out and be dissolved in the reaction medium when the pH is below 6 due to the HCl, which is able to dissolve the zinc oxide [72]. The high stability of these thin films can be explained by the high adhesion to the glass substrate due to the synthesis method used as well as the high chemical resistance of ZnO [73].

3.3. Antibacterial activity of transparent ZnO thin films

The antibacterial activity of thin ZnO films was tested, after UV irradiation for 3 h, using a standard method (JIS Z 2801_2000) developed for hard surfaces, such as glass. Glass samples were used as reference samples. Also, to evaluate the effect of UV irradiation, tests were conducted under UV light and in the dark, for the same testing time. After counting the viable cells that were recovered from the surface of the samples, the antibacterial rates were calculated. Results are presented in Fig. 8. First, glass and ZnO thin films were compared for any possible antibacterial effect in the dark. Bacterial counts obtained for the two types of samples showed no significantly different antibacterial properties (Fig. 8A). However, after testing the presence of UV light, a significant reduction in cell viability was observed for both samples (Fig. 8A). The samples, however, showed significantly different behaviours, with a 43.7 and 60.6% reduction in bacterial cells for glass and ZnO thin film, respectively. Results overall show that, when compared with glass surfaces, ZnO thin films make a significant addition to the antibacterial effect induced by UV irradiation of about 17% (Fig. 8B).

ZnO nanoparticles in general are described has posing noticeable antibacterial activities [74]. This activity is thought to be caused by the production of ROS, particularly in the presence of light. Also, other effects are possible, like causing membrane damage by accumulation on the cell's surface, by cell internalization or through Zn^{+} ion release [75]. In this work, thin films produced are not expected to release Zn^{+} ions. Possible mechanism of antibacterial action must therefore come from ROS generation and cell membrane damage, through ZnO thin film contact. The fact that no significant differences were found between glass and thin films, under dark conditions, may imply that, considering the experiment conditions, cell membrane damage and ROS generation were not effective. But, when testing the same samples after UV exposure, bacterial reduction was observed in both, but significantly greater in thin films. For glass samples, the reduction observed must be due to UV induced damages in membranes, proteins and DNA that affect general cellular processes [76]. The augmented antibacterial activity seen for ZnO thin films can be explained by the combined action with UV causing enhanced ROS generation, toxic to the cells. Synergistic effects to enhance photocatalytic activity of ZnO have already been reported [74]. To the best of our knowledge this is the first evidence obtained on ZnO transparent films holding strong promises of future applications, where additional antimicrobial properties are desired.

Table 2
ICP-OES results of the amount of zinc leached after the leaching screen experiments.

pH = 1				
Parameters	Test method	Analytical technique	Result	Units
Zn	Internal method based on ISO 11885	ICP-OES	4826	μg/L
pH = **7**				
Zn	Internal method based on ISO 11885	ICP-OES	<1	μg/L
pH = **14**				
Zn	Internal method based on ISO 11885	ICP-OES	<1	μg/L

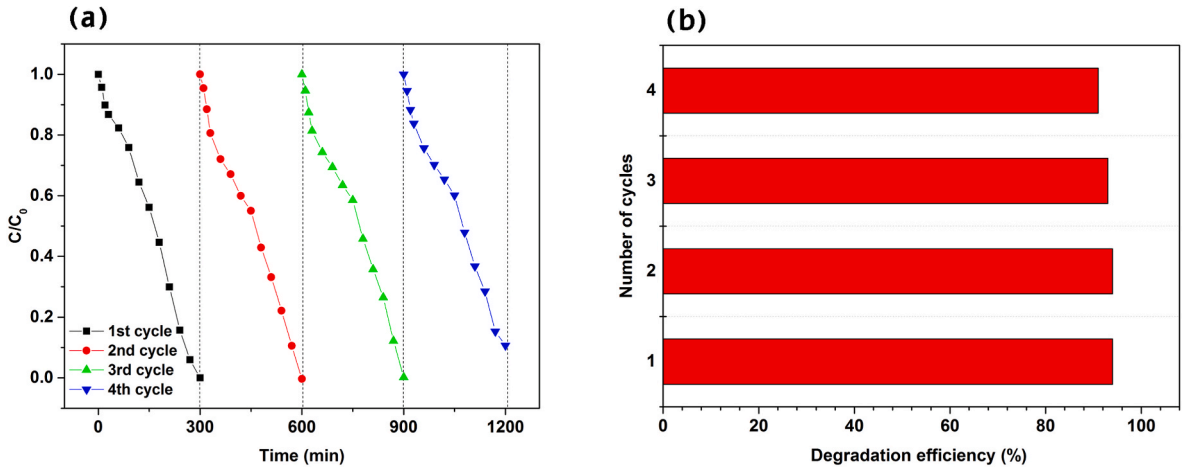

Fig. 7. (A) Reusability of the thin films in the photocatalytic degradation of 4-NP under UV light irradiation after a total of four cycles, and (b) a bar graph illustrating the percentage of degradation efficiency over four cycles.

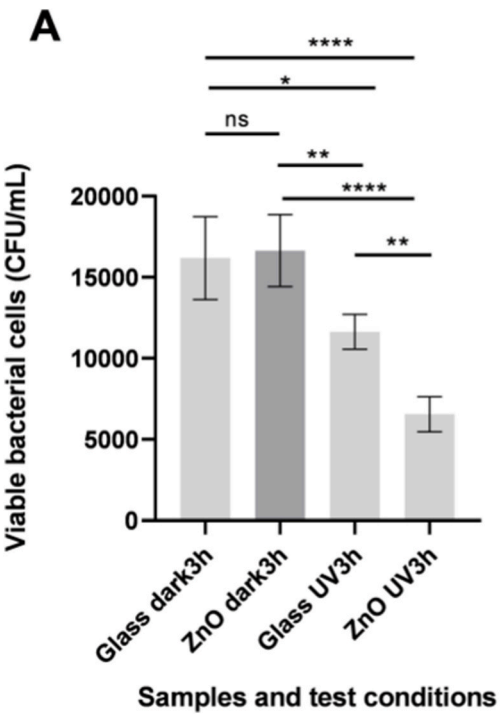

B

Samples	R (%)
Glass UV3h vs ZnO UV3h	43.7
ZnO dark3h vs ZnO UV3h	60.6

Fig. 8. Antibacterial evaluation of ZnO thin films: (A) Results of colony-forming units per millilitre (CFU/mL) in each sample tested. The significance of the results was determined using one-way ANOVA followed by Tukey's test for multiple comparisons. (B) Antibacterial rates (R) obtained for ZnO thin films compared to glass under UV light and to ZnO samples under dark and UV light.

4. Conclusion

This work presents a simple method of obtaining transparent ZnO thin films on glass, exhibiting an exceptional degree of transparency – over 95%. These thin films have been fabricated to act as photocatalysts for the degradation of water pollutants and bacteria. It is observed that their stability of these thin films is very high in neutral and basic aqueous media, thanks to the high adhesion of these films to the glass and the high chemical stability of ZnO. It has been shown that these films can generate hydroxyl radicals (OH•) when they are exposed to UV irradiation. The thin films exhibited high photocatalytic activity with 94% of 4-NP degraded after 270 min. The same catalyst was used for 4 degradation cycles maintaining an activity of 90% in the photo4-NP degradation. Comparing the reduction produced by a UV lamp when irradiating normal functionalized glass with these transparent ZnO layers, it was also discovered that radicals increase bacterial cell reduction by 17%. In future investigations, the evaluation of incorporating nanoparticles (NPs) onto the surface of these transparent thin films, along with the assessment of the films' photocatalytic activity under different light sources (such as visible light or sunlight), can be considered.

Declaration of competing interest

The authors declare that they have no known competing financial interests or personal relationships that could have appeared to influence the work reported in this paper.

Acknowledgements

The Ministry of Economy and Competitiveness (Spain), through the Ministry of Science, granted financial support under the identification MCIN/EAI/10.13039/501100011033 for project PID2020-116719RB-C43. This study was conducted as part of the projects UIDB/50011/2020, UIDP/50011/2020, and LA/P/0006/2020 at the CICECO-Aveiro Institute of Materials, which received backing from national funds through FCT/MCTES (PIDDAC). Ana C. Estrada expresses gratitude for the research contract funded by FCT, I.P., where the expenses were covered by national funds (OE) through FCT, as outlined in Article 23, points 4, 5, and 6 of Decree-Law 57/2016, amended by Law 57/2017. CESAM (UIDP/50017/2020 + UIDB/50017/2020 + LA/P/0094/2020) and CFE (UIDB/04004/2020) also received financial support from FCT/MCTES through national funds.

Appendix A. Supplementary data

Supplementary data to this article can be found online at https://doi.org/10.1016/j.ceramint.2023.07.246.

References

[1] F. Maiwald, S. Englmaier, S. Hierl, Absorber-free laser transmission welding of transparent polymers using fixed focus optics and 3D laser scanner, Procedia CIRP 94 (2020) 686–690, https://doi.org/10.1016/j.procir.2020.09.117.
[2] Y. Ming, Y. Sun, X. Liu, X. Liu, Y. Wu, Optical evaluation of a smart transparent insulation material for window application, Energy Convers. Manag. X. 16 (2022), 100315, https://doi.org/10.1016/j.ecmx.2022.100315.
[3] M. Chutturi, S. Gillela, S.M. Yadav, E.S. Wibowo, K. Sihag, S.M. Rangppa, P. Bhuyar, S. Siengchin, P. Antov, L. Kristak, A. Sinha, A comprehensive review of the synthesis strategies, properties, and applications of transparent wood as a renewable and sustainable resource, Sci. Total Environ. 864 (2023), 161067, https://doi.org/10.1016/j.scitotenv.2022.161067.
[4] D.S. Kim, J.Y. Jung, S. Seo, J.H. Kim, Facile fabrication of multifunctional transparent electrodes via spray deposition of indium-tin-oxide nanoparticles, Appl. Surf. Sci. 611 (2023), 155756, https://doi.org/10.1016/j.apsusc.2022.155756.
[5] E.S. Park, D.Y. Kim, J.H. Lee, J.U. Hwang, Y.S. Song, K.H. Park, H.J. Choi, Optical and electrical properties of amorphous alloy metal mesh for transparent flexible electrodes, Appl. Surf. Sci. 547 (2021), 149109, https://doi.org/10.1016/j.apsusc.2021.149109.
[6] Ryo Morita, Takayuki Nonoyama, Daisuke Abo, Takeshi Soyama, Noriyuki Fujima, Tetsuaki Imai, Hiroyuki Hamaguchi, Takuto Kameda, Osamu Sugita, Bunya Takahashi, Naoya Kinota, Kohsuke Kudo, Mechanical properties of a 3 dimensional–printed transparent flexible resin used for vascular model simulation compared with those of porcine arteries, J. Vasc. Intervent. Radiol. 34 (Issue 5) (2023) 871–878, https://doi.org/10.1016/j.jvir.2023.01.008, e3,ISSN 1051-0443.

[7] M.S.S. Hashuro, S. Tupin, N.K. Putra, K. Daibo, K. Inoue, T. Ishii, H. Kosukegawa, K. Funamoto, T. Hayase, M. Ohta, Development of ultrasound phantom made of transparent material: feasibility of optical particle image velocimetry, Ultrasound Med. Biol. 49 (6) (2023 Jun) 1385–1394, https://doi.org/10.1016/j.ultrasmedbio.2022.12.020.
[8] M.S. Kim, Y. Ahn, B.G. Kim, Improvement of scratch resistance in transparent hard surfaces through layer-by-layer coating, Prog. Org. Coating 170 (2022), 106991, https://doi.org/10.1016/j.porgcoat.2022.106991.
[9] W. Gao, F. Ma, Y. Yin, J. Li, Robust and durable transparent superhydrophobic F-TNTs/TiN coating fabricated by structure tuning on surface of TiN hard coating, Appl. Surf. Sci. 613 (2023), 155967, https://doi.org/10.1016/j.apsusc.2022.155967.
[10] O.J. Akinribide, G.N. Mekgwe, S.O. Akinwamide, F. Gamaoun, C. Abeykoon, O. T. Johnson, P.A. Olubambi, A review on optical properties and application of transparent ceramics, J. Mater. Res. Technol. 21 (2022) 712–738, https://doi.org/10.1016/j.jmrt.2022.09.027.
[11] A. Macková, A. Jagerová, O. Lalik, R. Mikšová, D. Poustka, J. Mistrík, V. Holý, J. D. Schutter, U. Kentsch, P. Marvan, A. Azarov, A. Galeckas, Combined Au/Ag nanoparticle creation in ZnO nanopillars by ion implantation for optical response modulation and photocatalysis, Appl. Surf. Sci. 610 (2023), 155556, https://doi.org/10.1016/j.apsusc.2022.155556. ISSN 0169-4332.
[12] Z.S. Shaymardanov, B.N. Rustamova, R. Jalolov, S.Z. Urolov, Influence of the nature of defects in zno nanocrystals synthesized by chemical bath deposition on photocatalytic activity, SSRN Electron. J. 649 (2022), 414444, https://doi.org/10.2139/ssrn.4211253.
[13] A. Bakour, A. Saadoune, I. Bouchama, F. Dhiabi, S. Boudour, M.A. Saeed, Effect and optimization of ZnO layer on the performance of GaInP/GaAs tandem solar cell, Micro and Nanostructures 168 (2022), 207294, https://doi.org/10.1016/j.micrna.2022.207294.
[14] S. Yang, H. Yu, The modification of ZnO surface with natural antioxidants to fabricate highly efficient and stable inverted organic solar cells, Chem. Eng. J. 452 (2023), 139658, https://doi.org/10.1016/j.cej.2022.139658.
[15] N.L. Marana, S. Casassa, J.R. Sambrano, Piezoelectricity induced by gaseous molecules adsorbed on ZnO nanotubes, Mater. Sci. Eng. B Solid-State Mater. Adv. Technol. 281 (2022), 115729, https://doi.org/10.1016/j.mseb.2022.115729.
[16] S. Cao, H. Zou, B. Jiang, M. Li, Q. Yuan, Incorporation of ZnO encapsulated MoS2 to fabricate flexible piezoelectric nanogenerator and sensor, Nano Energy 102 (2022), 107635, https://doi.org/10.1016/j.nanoen.2022.107635.
[17] S. Ananthi, M. Kavitha, E. Ranjith Kumar, T. Prakash, R. Vandamar Poonguzhali, B. Ranjithkumar, A. Balamurugan, Ch Srinivas, D.L. Sastry, Investigation of physicochemical properties of ZnO nanoparticles for gas sensor applications, Inorg. Chem. Commun. 146 (2022), 110152, https://doi.org/10.1016/j.inoche.2022.110152. ISSN 1387-7003.
[18] H. Zhang, Z. Li, A. Yu, S. Nie, J. Yi, Detection of 2-ethyl hexanol and dioctyl phthalate with potentiometric sensor based on ordered ZnO nanorods sensing electrode, Mater. Lett. 330 (2023), 133330, https://doi.org/10.1016/j.matlet.2022.133330.
[19] D.J. da Silva, A. Duran, A.D. Cabral, F.L.A. Fonseca, R.F. Bueno, D.S. Rosa, Questioning ZnO, Ag, and Ag/ZnO nanoparticles as antimicrobial agents for textiles: do they guarantee total protection against bacteria and SARS-CoV-2? J. Photochem. Photobiol. B Biol. 234 (2022), 112538 https://doi.org/10.1016/j.jphotobiol.2022.112538.
[20] Z. Sayyar, H. Jafarizadeh-Malmiri, N. Beheshtizadeh, A study on the anticancer and antimicrobial activity of Curcumin nanodispersion and synthesized ZnO nanoparticles, Process Biochem. 121 (2022) 18–25, https://doi.org/10.1016/j.procbio.2022.06.033.
[21] Luiza A. Gusmão, Diego A. Peixoto, Juliane Z. Marinho, Fernanda C. Romeiro, Rosana F. Gonçalves, Elson Longo, A. Carlos, de Oliveira, Renata C. Lima, Alkali influence on ZnO and Ag-doped ZnO nanostructures formation using the microwave-assisted hydrothermal method for fungicidal inhibition, J. Phys. Chem. Solid. 158 (2021), 110234, https://doi.org/10.1016/j.jpcs.2021.110234. ISSN 0022-3697.
[22] M. Ali, X. Wang, U. Haroon, H.J. Chaudhary, A. Kamal, Q. Ali, M.H. Saleem, K. Usman, A. Alatawi, S. Ali, M.F. Hussain Munis, Antifungal activity of Zinc nitrate derived nano Zno fungicide synthesized from Trachyspermum ammi to control fruit rot disease of grapefruit, Ecotoxicol. Environ. Saf. 233 (2022), 113311, https://doi.org/10.1016/j.ecoenv.2022.113311.
[23] K.H. Park, G.D. Han, K.C. Neoh, T.S. Kim, J.H. Shim, H.D. Park, Antibacterial activity of the thin ZnO film formed by atomic layer deposition under UV-A light, Chem. Eng. J. 328 (2017) 988–996, https://doi.org/10.1016/j.cej.2017.07.112.
[24] D. Sudha, E. Ranjith Kumar, S. Shanjitha, Alaa M. Munshi, Gamil A.A. Al-Hazmi, Nashwa M. El-Metwaly, S. Jone Kirubavathy, Structural, optical, morphological and electrochemical properties of ZnO and graphene oxide blended ZnO nanocomposites, Ceram. Int. 49 (Issue 5) (2023) 7284–7288, https://doi.org/10.1016/j.ceramint.2022.10.192. ISSN 0272-8842.
[25] S. Shabbir Awan, R. Taj Khan, A. Mehmood, M. Hafeez, S. Rizwan Abass, M. Nazir, M. Raffi, *Ailanthus altissima* leaf extract mediated green production of zinc oxide (ZnO) nanoparticles for antibacterial and antioxidant activity, Saudi J. Biol. Sci. 30 (1) (2023 Jan), 103487, https://doi.org/10.1016/j.sjbs.2022.103487.
[26] J. Žigon, U.G. Centa, M. Remškar, M. Humar, Application and characterization of a novel PVDF-HFP/PVP polymer composite with MoO3 nanowires as a protective coating for wood, Sci. Rep. 13 (1) (2023 Mar 1) 3429, https://doi.org/10.1038/s41598-023-30622-y.
[27] Y. Tu, X. Xiao, Y. Dong, J. Li, Y. Liu, Q. Zong, Y. Yuan, Cinnamaldehyde-based poly (thioacetal): a ROS-awakened self-amplifying degradable polymer for enhanced cancer immunotherapy, Biomaterials 289 (2022), 121795, https://doi.org/10.1016/j.biomaterials.2022.121795.
[28] Y. Zhang, M. Zhou, H. Cheng, S. Luo, Q. Sun, Insight into the substrate-dependent anti-aflatoxigenic effects of nanosized ZnO film: electron transfer directed oxidative stress mechanisms, Colloids Surf. B Biointerfaces 207 (2021), 111997, https://doi.org/10.1016/j.colsurfb.2021.111997.
[29] H. Hong, Z. Liu, S. Li, D. Wu, L. Jiang, P. Li, Z. Wu, J. Xu, A. Jiang, Y. Zhang, Z. Wei, Z. Yang, Zinc oxide nanoparticles (ZnO-NPs) exhibit immune toxicity to crucian carp (Carassius carassius) by neutrophil extracellular traps (NETs) release and oxidative stress, Fish Shellfish Immunol. 129 (2022) 22–29, https://doi.org/10.1016/j.fsi.2022.07.025.
[30] M. Mancinelli, C. Stevanin, M. Ardit, T. Chenet, L. Pasti, A. Martucci, PFAS as emerging pollutants in the environment: a challenge with FAU type and silver-FAU exchanged zeolites for their removal from water, J. Environ. Chem. Eng. 10 (2022), 108026, https://doi.org/10.1016/j.jece.2022.108026.
[31] European Chemicals Agency, ECHA (the European chemicals agency), in: Philip Wexler (Ed.), Encyclopedia of Toxicology(ThirdEdition), Academic Press, 2014, pp. 263–264, https://doi.org/10.1016/B978-0-12-386454-3.00551-0, 9780123864550.
[32] J.B. Feng, Y. yuan Li, Y. Zhang, Y. yin Xu, X.W. Cheng, Adsorptive removal of indomethacin and diclofenac from water by polypyrrole doped-GO/COF-300 nanocomposites, Chem. Eng. J. 429 (2022), 132499, https://doi.org/10.1016/j.cej.2021.132499.
[33] J. Mcginley, M.G. Healy, P.C. Ryan, H.O. Driscoll, P. Mellander, L. Morrison, A. Siggins, Science of the Total Environment Impact of historical legacy pesticides on achieving legislative goals in Europe, Sci. Total Environ. 873 (2023), 162312, https://doi.org/10.1016/j.scitotenv.2023.162312.
[34] K. Nozaki, R. Tanoue, T. Kunisue, N.M. Tue, S. Fujii, N. Sudo, T. Isobe, K. Nakayama, A. Sudaryanto, A. Subramanian, K.A. Bulbule, P. Parthasarathy, L. H. Tuyen, P.H. Viet, M. Kondo, S. Tanabe, K. Nomiyama, Pharmaceuticals and personal care products (PPCPs) in surface water and fish from three Asian countries: species-specific bioaccumulation and potential ecological risks, Sci. Total Environ. 866 (2023), 161258, https://doi.org/10.1016/j.scitotenv.2022.161258.
[35] L.B.B. Ndong, M.P. Ibondou, Z. Miao, X. Gu, S. Lu, Z. Qiu, Q. Sui, S.M. Mbadinga, Efficient dechlorination of chlorinated solvent pollutants under UV irradiation by using the synthesized TiO2 nano-sheets in aqueous phase, J. Environ. Sci. 26 (2014) 1188–1194, https://doi.org/10.1016/S1001-0742(13)60541-0.
[36] A.A. Essawy, I.B. Abdel-Farid, Hybrid solvothermal/sonochemical-mediated synthesis of ZnO NPs generative of [rad]OH radicals: photoluminescent approach to evaluate [rad]OH scavenging activity of Egyptian and Yemeni Punica granatum arils extract, Ultrason. Sonochem. 89 (2022), 106152, https://doi.org/10.1016/j.ultsonch.2022.106152.
[37] M.N. Rezaie, S. Mohammadnejad, S. Ahadzadeh, The impact of ZnO nanotube on the performance of hybrid inorganic/organic light-emitting diode as a single-mode ring-core UV waveguide, Surface. Interfac. 28 (2022), 101666, https://doi.org/10.1016/j.surfin.2021.101666.
[38] B.J. Lee, S. Il Jo, S.G. Heo, W.Y. Lee, G.H. Jeong, Structure-controllable synthesis of ZnO nanowires using water vapor in an atmospheric-pressure microwave plasma system, Curr. Appl. Phys. 28 (2021) 52–58, https://doi.org/10.1016/j.cap.2021.05.004.
[39] L. Demelius, M. Blatnik, K. Unger, P. Parlanti, M. Gemmi, A.M. Coclite, Shedding light on the initial growth of ZnO during plasma-enhanced atomic layer deposition on vapor-deposited polymer thin films, Appl. Surf. Sci. 604 (2022), 154619, https://doi.org/10.1016/j.apsusc.2022.154619.
[40] P.P. Fu, Q. Xia, H.M. Hwang, P.C. Ray, H. Yu, Mechanisms of nanotoxicity: generation of reactive oxygen species, J. Food Drug Anal. 22 (2014) 64–75, https://doi.org/10.1016/j.jfda.2014.01.005.
[41] J.G. Cuadra, L. Scalschi, B. Vicedo, M. Guc, V. Izquierdo-Roca, S. Porcar, D. Fraga, J.B. Carda, ZnO/Ag nanocomposites with enhanced antimicrobial activity, Appl. Sci. 12 (2022) 5023, https://doi.org/10.3390/app12105023.
[42] B. Jaleh, S. Hamzehi, R. Sepahvand, S. Azizian, M. Eslamipanah, R. Golbedaghi, A. Meidanchi, R. Fausto, Preparation of polycarbonate-ZnO nanocomposite films: surface investigation after UV irradiation, Molecules 27 (14) (2022 Jul 12) 4448, https://doi.org/10.3390/molecules27144448.
[43] Ammar Nayfeh, Nazek El-Atab, 6 - agglomeration-based nanoparticle fabrication, in: Ammar Nayfeh, Nazek El-Atab (Eds.), Micro and Nano Technologies, Nanomaterials-Based Charge Trapping Memory Devices, Elsevier, 2020, pp. 133–153, https://doi.org/10.1016/B978-0-12-822342-0.00006-7, 9780128223420.
[44] Alfina Grasso, Margherita Ferrante, Antonio Moreda-Piñeiro, Giovanni Arena, Riccardo Magarini, Gea Oliveri Conti, Antonio Cristaldi, Chiara Copat, Dietary exposure of zinc oxide nanoparticles (ZnO-NPs) from canned seafood by single particle ICP-MS: balancing of risks and benefits for human health, Ecotoxicol. Environ. Saf. 231 (2022), 113217, https://doi.org/10.1016/j.ecoenv.2022.113217. ISSN 0147-6513.
[45] L. Liu, H. Nian, T. Lian, Plants and rhizospheric environment: affected by zinc oxide nanoparticles (ZnO NPs). A review, Plant Physiol. Biochem. 185 (2022) 91–100, https://doi.org/10.1016/j.plaphy.2022.05.032.
[46] S.W. Bian, I.A. Mudunkotuwa, T. Rupasinghe, V.H. Grassian, Aggregation and dissolution of 4 nm ZnO nanoparticles in aqueous environments: influence of pH, ionic strength, size, and adsorption of humic acid, Langmuir 27 (2011) 6059–6068, https://doi.org/10.1021/la200570n.
[47] S.Y. Lee, D. Park, B.S. Yoon, Y.S. Lee, Y. Il Park, C.H. Ko, Atomic layer deposition-based synthesis of TiO2 and Al2O3 thin-film coatings on nanoparticle powders for

sodium-ion batteries with enhanced cyclic stability, J. Alloys Compd. 897 (2022), 163113, https://doi.org/10.1016/j.jallcom.2021.163113.
[48] S.I. Dorovskikh, D.D. Klyamer, A.M. Makarenko, K.V. Zherikova, A. E. Turgambaeva, Y.V. Shevtsov, D.B. Kal'nyi, I.K. Igumenov, N.B. Morozova, The comprehensive study of thermal properties of tris(2,2,6,6-tetramethyl-3,5-heptanedionato)cobalt(III) related to the chemical vapor deposition of Co-oxide based thin film materials, Vacuum 199 (2022), 110969, https://doi.org/10.1016/j.vacuum.2022.110969.
[49] V.T. Lukong, R.T. Mouchou, G.C. Enebe, K. Ukoba, T.C. Jen, Deposition and characterization of self-cleaning TiO2 thin films for photovoltaic application, Mater. Today Proc. (2022), https://doi.org/10.1016/j.matpr.2022.02.089.
[50] R.S. Santiago, L.C.D. Silva, F.D. Origo, C. Stegemann, I.L. Graff, R.G. Delatorre, D. A. Duarte, Target power influence on optical and electrical properties of amorphous titanium oxide deposited by reactive grid-assisted magnetron sputtering, Thin Solid Films 700 (2020), 137917, https://doi.org/10.1016/j.tsf.2020.137917. ISSN 0040-6090.
[51] K. Vijayan, S.P. Vijayachamundeeswari, K. Sivaperuman, N. Ahsan, T. Logu, Y. Okada, A review on advancements, challenges, and prospective of copper and non-copper based thin-film solar cells using facile spray pyrolysis technique, Sol. Energy 234 (2022) 81–102, https://doi.org/10.1016/j.solener.2022.01.070.
[52] A.L. Patterson, The scherrer formula for X-ray particle size determination, Phys. Rev. 56 (1939) 978–982, https://doi.org/10.1103/PhysRev.56.978.
[53] T. Ratana, P. Amornpitoksuk, T. Ratana, S. Suwanboon, The wide band gap of highly oriented nanocrystalline Al doped ZnO thin films from sol-gel dip coating, J. Alloys Compd. 470 (2009) 408–412, https://doi.org/10.1016/j.jallcom.2008.02.081.
[54] J.T. Schneider, D.S. Firak, R.R. Ribeiro, P. Peralta-Zamora, Use of scavenger agents in heterogeneous photocatalysis: truths, half-truths, and misinterpretations, Phys. Chem. Chem. Phys. 22 (2020) 15723–15733, https://doi.org/10.1039/d0cp02411b.
[55] T. Liu, L. Wang, X. Lu, J. Fan, X. Cai, B. Gao, R. Miao, J. Wang, Y. Lv, Comparative study of the photocatalytic performance for the degradation of different dyes by ZnIn2S4: adsorption, active species, and pathways, RSC Adv. 7 (2017) 12292–12300, https://doi.org/10.1039/c7ra00199a.
[56] J.G. Cuadra, S. Molina-Prados, G. Mínguez-Vega, A.C. Estrada, T. Trindade, C. Oliveira, M.P. Seabra, J. Labrincha, S. Porcar, R. Cadena, D. Fraga, J.B. Carda, Multifunctional silver-coated transparent TiO2 thin films for photocatalytic and antimicrobial applications, Appl. Surf. Sci. 617 (2023), 156519, https://doi.org/10.1016/j.apsusc.2023.156519.
[57] X. Bai, B. Sun, X. Wang, T. Zhang, Q. Hao, B.J. Ni, R. Zong, Z. Zhang, X. Zhang, H. Li, Defective crystal plane-oriented induced lattice polarization for the photocatalytic enhancement of ZnO, CrystEngComm 22 (2020) 2709–2717, https://doi.org/10.1039/c9ce01966a.
[58] S.H. Ribut, C.A. Che Abdullah, M.Z. Mohammad Yusoff, Investigations of structural and optical properties of zinc oxide thin films growth on various substrates, Results Phys. 13 (2019), 102146, https://doi.org/10.1016/j.rinp.2019.02.082.
[59] R. Cuscó, E. Alarcón-Lladó, J. Ibáñez, L. Artús, J. Jiménez, B. Wang, M.J. Callahan, Temperature dependence of Raman scattering in ZnO, Phys. Rev. B Condens. Matter 75 (2007) 1–11, https://doi.org/10.1103/PhysRevB.75.165202.
[60] H. Ali, A.M. Alsmadi, B. Salameh, M. Mathai, M. Shatnawi, N.M.A. Hadia, E.M. M. Ibrahim, Influence of nickel doping on the energy band gap, luminescence, and magnetic order of spray deposited nanostructured ZnO thin films, J. Alloys Compd. 816 (2020), 152538, https://doi.org/10.1016/j.jallcom.2019.152538.
[61] M.R. Al Hassan, Asrafuzzaman, M.A. Islam, K. Salam, K.F. Amin, M.K. Hasan, Synthesis of spray deposited transition metals doped (Cr, Mn, Fe, Ni, and Cu) compositionally complex ZnO thin films with enhanced band gap and magnetism, Results Mater 13 (2022), https://doi.org/10.1016/j.rinma.2022.100263.
[62] C. Jin, X. Yang, X. Zhai, S. Wang, W. Zhang, Applied Surface Science ZnO/Sn 3 O 4 amorphous-crystalline heterojunctions for Cr (VI) visible photocatalysis: simple synthesis with excellent performance, Appl. Surf. Sci. 608 (2023), 155263, https://doi.org/10.1016/j.apsusc.2022.155263.
[63] L. Zhang, B. Liang, H. Zhao, J. Yang, M. Jiao, Y. Liu, Core-shell structured ZnO homojunction for enhanced photocatalysis, Inorg. Chem. Commun. 148 (2023), 110281, https://doi.org/10.1016/j.inoche.2022.110281.
[64] R.D. Suryavanshi, S.V. Mohite, A.A. Bagade, S.K. Shaikh, J.B. Thorat, K.Y. Rajpure, Nanocrystalline immobilised ZnO photocatalyst for degradation of benzoic acid and methyl blue dye, Mater. Res. Bull. 101 (2018) 324–333, https://doi.org/10.1016/j.materresbull.2018.01.042. ISSN 0025-5408.
[65] A. Fertier, A. Montarnal, S. Truptil, F. Bénaben, Jo ur na l P re Jo ur l P re, Decis. Support Syst. (2020), 113260, https://doi.org/10.1016/j.ceramint.2023.03.024.
[66] Y. Hu, L. Sun, Z. Liu, T. Liu, Controlled solvothermal synthesis of ZnO nanoparticles using non-destructive Mg-based channel templates for enhanced photocatalytic performance, Mater. Chem. Phys. 299 (2023), 127525, https://doi.org/10.1016/j.matchemphys.2023.127525.
[67] J. Zheng, Z.J. Ã, Q.K. Ã, Z. Xie, R. Huang, L. Zheng, Journal of Solid State Chemistry Shape-controlled fabrication of porous ZnO architectures and their photocatalytic properties 182 (2009) 115–121, https://doi.org/10.1016/j.jssc.2008.10.009.
[68] Subrata Naskar, S. Arumugom Pillay, Manas Chanda, Photocatalytic degradation of organic dyes in aqueous solution with TiO2 nanoparticles immobilized on foamed polyethylene sheet, J. Photochem. Photobiol. Chem. 113 (Issue 3) (1998) 257–264, https://doi.org/10.1016/S1010-6030(97)00258-X. ISSN 1010-6030.
[69] Dingwang Chen, Ajay K. Ray, Photodegradation kinetics of 4-nitrophenol in TiO2 suspension, Water Res. 32 (Issue 11) (1998) 3223–3234, https://doi.org/10.1016/S0043-1354(98)00118-3. ISSN 0043-1354.
[70] N. Daneshvar, M.A. Behnajady, Y. Zorriyeh Asghar, Photooxidative degradation of 4-nitrophenol (4-NP) in UV/H2O2 process: influence of operational parameters and reaction mechanism, J. Hazard Mater. 139 (2007) 275–279, https://doi.org/10.1016/j.jhazmat.2006.06.045.
[71] Guanhua Zhang, Jieyi Yang, Zhiling Huang, Guoxiang Pan, Bo Xie, Zheming Ni, Shengjie Xia, Construction dual vacancies to regulate the energy band structure of ZnIn2S4 for enhanced visible light-driven photodegradation of 4-NP, J. Hazard Mater. 441 (2023), 129916, https://doi.org/10.1016/j.jhazmat.2022.129916. ISSN 0304-3894.
[72] Gerd Brunner, Chapter 3 - properties of mixtures with water, in: Gerd Brunner (Ed.), Supercritical Fluid Science and Technology, vol. 5, Elsevier, 2014, pp. 95–225, https://doi.org/10.1016/B978-0-444-59413-6.00003-0. ISSN 2212-0505,ISBN 9780444594136.
[73] R. Saidi, K. Raeissi, F. Ashrafizadeh, M. Kharaziha, The effect of zinc oxide coating morphology on corrosion performance of Ti-6Al-4 V alloys, J. Alloys Compd. 883 (2021), 160771, https://doi.org/10.1016/j.jallcom.2021.160771.
[74] K. Qi, B. Cheng, J. Yu, W. Ho, Review on the improvement of the photocatalytic and antibacterial activities of ZnO, J. Alloys Compd. 727 (2017) 792–820, https://doi.org/10.1016/j.jallcom.2017.08.142.
[75] A.B. Djurišić, X. Chen, Y.H. Leung, A. Man Ching Ng, ZnO nanostructures: growth, properties and applications, J. Mater. Chem. 22 (2012) 6526–6535, https://doi.org/10.1039/c2jm15548f.
[76] F. Vatansever, C. Ferraresi, M.V.P. de Sousa, R. Yin, A. Rineh, S.K. Sharma, M. R. Hamblin, Can biowarfare agents be defeated with light? Virulence 4 (2013) 796–825, https://doi.org/10.4161/viru.26475.